



## Planforms of self-consistently generated plates in 3D spherical geometry

H. J. van Heck<sup>1</sup> and P. J. Tackley<sup>1</sup>

Received 22 July 2008; revised 4 September 2008; accepted 5 September 2008; published 14 October 2008.

[1] In the past decade, several studies have documented the effectiveness of plastic yielding in causing a basic approximation of plate tectonic behavior in mantle convection models with strongly temperature dependent viscosity, strong enough to form a rigid lid in the absence of yielding. The vast majority of such research to date has been in either two-dimensional, or three-dimensional cartesian geometry. In the present study, mantle convection calculations are performed to investigate the planform of self-consistent tectonic plates in three-dimensional spherical geometry. The results are compared to those of similar calculations where a three dimensional cartesian geometry is used. We found that when yield stress of the lithosphere is low ( $\sim 20$  MPa) a “great circle”-subduction zone forms. At low-intermediate yield stresses ( $\sim 100$  MPa) plates, spreading centers and subduction zones formed and were destroyed over time. At high-intermediate yield stresses ( $\sim 200$  MPa) two plates form, separated by a great circle boundary that is a spreading centre on one side and a subduction zone on the other side. At high yield stresses ( $\sim 400$  MPa) a rigid lid was observed. The great circle subduction zone and the rigid lid are stable over time while at intermediate yield stresses some episodic behavior is observed. The spherical cases showed a higher, more Earth-like, toroidal-poloidal ratio of the surface velocity field than the cartesian cases. **Citation:** van Heck, H. J., and P. J. Tackley (2008), Planforms of self-consistently generated plates in 3D spherical geometry, *Geophys. Res. Lett.*, 35, L19312, doi:10.1029/2008GL035190.

### 1. Introduction

[2] As oceanic plates act as the upper thermal boundary layer of mantle convection, and continents are formed from the mantle, it is desirable to treat mantle and plates as a single, integrated system rather than two separate entities. The physics of the formation and destruction of tectonic plates out of a convecting mantle is, however, not well understood.

[3] Although in recent years progress has been made in both the comprehensiveness and clarity of numerical models (see *Bercovici* [2003] for a review) basic questions about why the Earth is currently the only terrestrial planet with active plate tectonics, which parameters control the formation of plates, and which processes are responsible for the

creation of subduction zones and spreading centers, remain largely unanswered.

[4] Convection with temperature dependent viscosity displays three different regimes, none of which is plate like. *Solomatov* [1995] and *Moresi and Solomatov* [1995] conducted numerical experiments of convection with large viscosity contrasts. They found distinct different regimes in which the top part did or did not participate in convection, separating a rigid lid regime from a mobile and a sluggish lid regime. Models got much closer to modeling plate-like behavior when *Moresi and Solomatov* [1998] introduced a lithospheric yield stress. When stresses exceed a certain critical stress, the lithosphere is weakened by yielding, modeling faults and shear zones. This approach was used in 3D cartesian geometry by *Trompeter and Hansen* [1998] and *Tackley* [2000a]. In general, these studies found three distinctive convective regimes: mobile lid, where the lithosphere is constantly yielding, allowing zones of subduction and spreading centres to be present at all times, a stagnant lid, where one continuous plate covers the whole domain, and episodic lid, where the regime keeps changing from mobile lid to stagnant lid, back to mobile lid over time. Later some studies included more Earth-like features such as history dependent weakening [*Tackley*, 2000b; *Ogawa*, 2003] and a low viscosity asthenosphere [*Tackley*, 2000b; *Richards et al.*, 2001]. *Stein et al.* [2004] used a similar but more extensive approach to study, among others, the influence of temperature, stress and pressure dependence of the viscosity on plate-like behavior. *Muhlhaus and Regenauer-Lieb* [2005] discussed the importance of elasticity and non-Newtonian rheology. Recently, *Loddoch et al.* [2006] argued that a fourth regime exists between the rigid and episodic lid, where different scalings apply. Not only the Earth’s dynamics but that of all terrestrial planets can be studied with these kind of models. For example, *Fowler and O’Brien* [2003] used a model similar to the ones mentioned above to investigate the frequency of resurfacing events on Venus.

[5] Of these studies, only *Richards et al.* [2001] showed results in spherical geometry, while the majority of these studies were done using cartesian geometry. How the different tectonic regimes manifest in 3D spherical geometry is not yet clear.

[6] Here we present the results of numerical experiments of mantle convection with self consistent plate tectonics in 3D spherical geometry. The results are compared to the results of calculations using the same parameter values in cartesian geometry. Special attention was paid to the effect of varying values of lithospheric yield stress, leading to comparable regimes as were observed in cartesian geometry

<sup>1</sup>Institute of Geophysics, ETH Zurich, Zurich, Switzerland.

[Tackley, 2000a], and the similarities and differences between cartesian and spherical geometries.

## 2. Model Description

### 2.1. Boussinesq Equations

[7] The same model is used as was used by Tackley [2000a], assuming the Boussinesq approximation. Solving the equations for conservation of mass, momentum and continuity;

$$\nabla \cdot \mathbf{v} = 0, \quad (1)$$

$$\nabla \cdot \boldsymbol{\sigma}_{ij} - \nabla p = RaT\hat{z}, \quad (2)$$

$$\frac{\partial T}{\partial t} = \nabla^2 T - \mathbf{v} \cdot \nabla T + H, \quad (3)$$

where  $\mathbf{v}$  is velocity,  $\boldsymbol{\sigma}_{ij}$  is the deviatoric stress tensor ( $= \eta(v_{i,j} + v_{j,i})$  where  $\eta$  is viscosity),  $p$  the pressure,  $T$  the temperature,  $\hat{z}$  the vertical unit vector,  $t$  the time, and  $H$  the internal heating rate. The Rayleigh number  $Ra$  can be expressed as:

$$Ra = \frac{\rho g \alpha \Delta T D^3}{\eta_0 \kappa}, \quad (4)$$

where  $\rho$ ,  $g$ ,  $\alpha$ ,  $\Delta T$ ,  $D$ ,  $\kappa$  and  $\eta_0$  are density, gravitational acceleration, temperature scale, depth of the mantle, thermal diffusivity and reference viscosity respectively.

### 2.2. Rheology

[8] The basic temperature dependent expression for the viscosity is an Arrhenius-type law:

$$\eta(T) = \exp \left[ \frac{23.03}{T+1} - \frac{23.03}{2} \right]. \quad (5)$$

This law results in a variation in viscosity of  $10^5$  between the nondimensional temperatures of 0 and 1. The viscosity is equal to 1 at  $T = 1$ .

[9] To account for plastic yielding we followed the method as described by Tackley [2000b], using a two component yield stress. One depth dependent component models brittle failure in the upper crust, and one constant component models semi-ductile, semi-brittle flow in the lower crust and mantle lithosphere.

$$\sigma_{\text{yield}}(z) = \min \left[ \sigma_{y\text{-ductile}}, (1-z)\sigma'_{y\text{-brittle}} \right], \quad (6)$$

where  $\sigma_{\text{yield}}$  is the depth dependent yield stress,  $\sigma_{y\text{-ductile}}$  the constant yield stress and  $\sigma'_{y\text{-brittle}}$  the gradient of the brittle yield stress with depth. The intersection was kept at a constant depth by using;  $\sigma'_{y\text{-brittle}} = 20 * \sigma_{y\text{-ductile}}$ , meaning that the upper five percent of the domain experiences the brittle yield stress while the rest of the domain experiences the ductile yield stress. These yielding criteria lead to a “yield viscosity”,  $\eta_{\text{yield}}$ :

$$\eta_{\text{yield}} = \frac{\sigma_{\text{yield}}(z)}{2\dot{\epsilon}}, \quad (7)$$

where  $\dot{\epsilon}$  is the second invariant of the strain rate tensor:

$$\dot{\epsilon} = \sqrt{\frac{1}{2} \dot{\epsilon}_{ij} \dot{\epsilon}_{ij}}. \quad (8)$$

[10] The effective viscosity was defined as:

$$\eta_{\text{eff}} = \frac{1}{\frac{1}{\eta(z,T)} + \frac{1}{\eta_{\text{yield}}}}, \quad (9)$$

resulting in a smooth transition from the basic depth and temperature dependent viscosity to the yield-viscosity in regions of high stress. To avoid numerical difficulties the viscosity was truncated between 0.1 and 10000.

[11] Richards *et al.* [2001] and Tackley [2000b] showed that a reduction in viscosity in the asthenosphere enhances plate formation. Viscosity reduction in the asthenosphere was here incorporated by reducing the viscosity by a factor of 10 in regions where the temperature is close to the solidus, i.e.,

$$\eta(z, T) = \eta(T) \quad \text{if } T < T_{\text{sol}0} + 2(1-z), \quad (10)$$

$$\eta(z, T) = 0.1\eta(T) \quad \text{if } T \geq T_{\text{sol}0} + 2(1-z), \quad (11)$$

where  $z$ , the depth coordinate, is varying from 0 at the core-mantle boundary (CMB) to 1 at the surface. The surface solidus temperature  $T_{\text{sol}0}$  was set to 0.6 in the calculations done, giving low viscosity regions mainly localized underneath spreading centers.

### 2.3. Plate Diagnostics

[12] To analyze how successful each model was at producing plate tectonics we used three diagnostics; plateness, mobility and the toroidal-poloidal ratio of the surface velocity field. The same diagnostics were used by Tackley [2000a, 2000b].

[13] Surface deformation should be localized in plate boundaries, leaving the plates themselves fairly rigid. “Plateness” ( $P$ ) is a parameter to indicate how localized surface deformation is, and can be expressed as:

$$P = 1 - \frac{f_{80}}{0.6}, \quad (12)$$

where  $f_{80}$  is the fraction of the surface area where the highest 80% of the surface deformation takes place. Deformation is measured by the second invariant of the strain rate tensor;

$$\dot{\epsilon}_{\text{surface}} = \sqrt{\dot{\epsilon}_{xx}^2 + \dot{\epsilon}_{yy}^2 + 2\dot{\epsilon}_{xy}^2}. \quad (13)$$

[14] The plateness is scaled to cases with constant viscosity which show a  $f_{80}$  of 0.6 (in both cartesian and spherical geometry). A plateness of 1 corresponds to perfect plates, i.e., 80% of the surface deformation is localized in an infinitesimal small area, while cases with constant viscosity show a plateness of 0.

[15] Mobility ( $M$ ) is defined as the ratio of rms surface velocity to rms velocity averaged over the entire domain:

$$M = \frac{v_{\text{rms-surface}}}{v_{\text{rms-whole}}}. \quad (14)$$

For constant viscosity, internally heated convection,  $M \approx 1$ .

[16] The Toroidal-poloidal ratio ( $R_{TP}$ ) is expressed as:

$$R_{TP} = \sqrt{\frac{v_{\text{toroidal}}^2}{v_{\text{poloidal}}^2}}, \quad (15)$$

where  $v_{\text{toroidal}}$  is the toroidal component of the surface velocity field averaged over the entire surface and  $v_{\text{poloidal}}$  the poloidal component averaged over the surface. The estimated value for the Earth is, without net rotation, 0.3–0.5 (for the past 120 My [*Lithgow-Bertelloni and Richards, 1993*]). Net rotation of the lithosphere is subtracted from the surface velocity field at each timestep [*Tackley, 2008*].

## 2.4. Parameters and Numerical Method

[17] The Rayleigh number was set to  $10^5$  (temperature based, viscosity for  $T = 1$ ). The cartesian cases used periodic boundaries and an aspect ratio of 8. Both on the surface and CMB free-slip boundary conditions were applied. The temperature at the surface was kept at 0, at the bottom zero heat flux was applied, i.e., all cases were completely heated from within.

[18] The internal heating was 10 in cartesian geometry, increased to 16.3 when switching to spherical geometry to compensate for the higher surface:volume ratio that spherical geometry has. With this increase, the surface heat flux is comparable in both geometries. The ratio surface:volume changes as:

$$[\text{surface:volume}]_{\text{cartesian}} = (r_{\text{surf}}) - (r_{\text{cmb}}), \quad (16)$$

$$[\text{surface:volume}]_{\text{spherical}} = \frac{3*(r_{\text{surf}})^2}{[(r_{\text{surf}})^3 - (r_{\text{cmb}})^3]}, \quad (17)$$

where  $r_{\text{surf}}$  is the radius of the Earth and  $r_{\text{cmb}}$  the radius of the Earth's core. Using  $r_{\text{surf}} = 2.2$  and  $r_{\text{cmb}} = 1.2$  gives  $[\text{surface:volume}]_{\text{cartesian}} = 1$  and  $[\text{surface:volume}]_{\text{spherical}} \approx 1.63$ .

[19] The initial condition used for each calculation was a stable rigid lid. From there, all calculations were ran for a time corresponding to several billion years.

[20] The latest version of the code Stag3d is used [*Tackley, 1993, 2000a*]. This code has recently been converted to spherical geometry using a yin-yang grid [*Tackley, 2008*]. The number of grid points was  $128 \times 128 \times 32$  for cartesian cases and  $64 \times 192 \times 32 \times 2$  for spherical cases. Resolution tests for the cartesian cases were published by *Tackley [2000b]*. We expect similar behavior for the spherical cases since the same code is used. One spherical test case was run with double resolution ( $128 \times 384 \times 64 \times 2$ ), which didn't show any significant changes. To check that the solutions were not influenced by the underlying grid we rotated the solution arbitrarily and continued the calculation

for one of the calculations done. A snapshot is shown in Figure 1.

## 3. Results

### 3.1. Varying Yield Stress

[21] Two sets of six calculations each are presented; one in cartesian geometry, the other in spherical geometry. In both sets the yield stress (both the brittle part and the ductile part) was varied over a range wide enough to create a rigid lid at the high end and a stable mobile lid at the low end.

[22] To convert non-dimensional stress values to dimensional values we use the expression;

$$\sigma_{\text{dimensional}} = \frac{\eta_0 \kappa}{D^2} \sigma_{\text{non-dimensional}}. \quad (18)$$

[23] When using the values shown in Table 1 it follows that a non-dimensional stress of 1 corresponds to a dimensional value of  $1.2 \times 10^4$  Pa (or  $10^4$  to 120 MPa).

[24] Figure 1 shows snapshots of the surface viscosity, surface velocity fields and an isosurface of the temperature field for all calculations. The yield stress increases from top to bottom from  $1.4 * 10^3$  to  $3.5 * 10^4$ , or 17 to 420 MPa. The observed planforms can be divided into four groups. 1) low yield stress. These planforms are dominated by two perpendicular downwellings in cartesian geometry and one "great circle downwelling" in spherical geometry (Figure 1, top row). The rest of the surface is filled by several higher viscosity "oceanic plates".

[25] 2) Low-intermediate yield stress. Spreading centers, subduction zones and oceanic plates form and are destroyed over time. A single planform can not be identified for this group (Figure 1, first through fourth rows).

[26] 3) High-intermediate yield stress. In cartesian geometry one upwelling and one downwelling form. Convection has the longest wavelength possible in the domain. In spherical geometry one elongated upwelling and one elongated downwelling form roughly opposite each other. Two hemispherical "oceanic plates" are formed (Figure 1, fifth row).

[27] 4) High yield stress. In both cartesian and spherical geometry a rigid lid forms in this group (Figure 1, bottom row.)

### 3.2. Plate Diagnostics

[28] In Figure 2 the plate diagnostics are plotted versus yield stress. Mobility holds a stable value with varying yield stress until it drops to almost zero when a rigid lid is formed. The value for the spherical cases ( $\sim 1.25$ ) is slightly lower than the value for the cartesian cases ( $\sim 1.45$ ). Plateness increases with yield stress and drops drastically when a rigid lid is formed, in a very similar way for the spherical and cartesian cases. The toroidal-poloidal ratio increases with yield stress at low yield stresses, then it drops until a rigid lid is formed. The toroidal-poloidal ratio is significantly higher for spherical cases than it is for cartesian cases, up to a factor of two for most cases.

## 4. Discussion and Conclusions

[29] The effect of 3D spherical geometry on the planforms of self-consistent plate tectonics is investigated. The

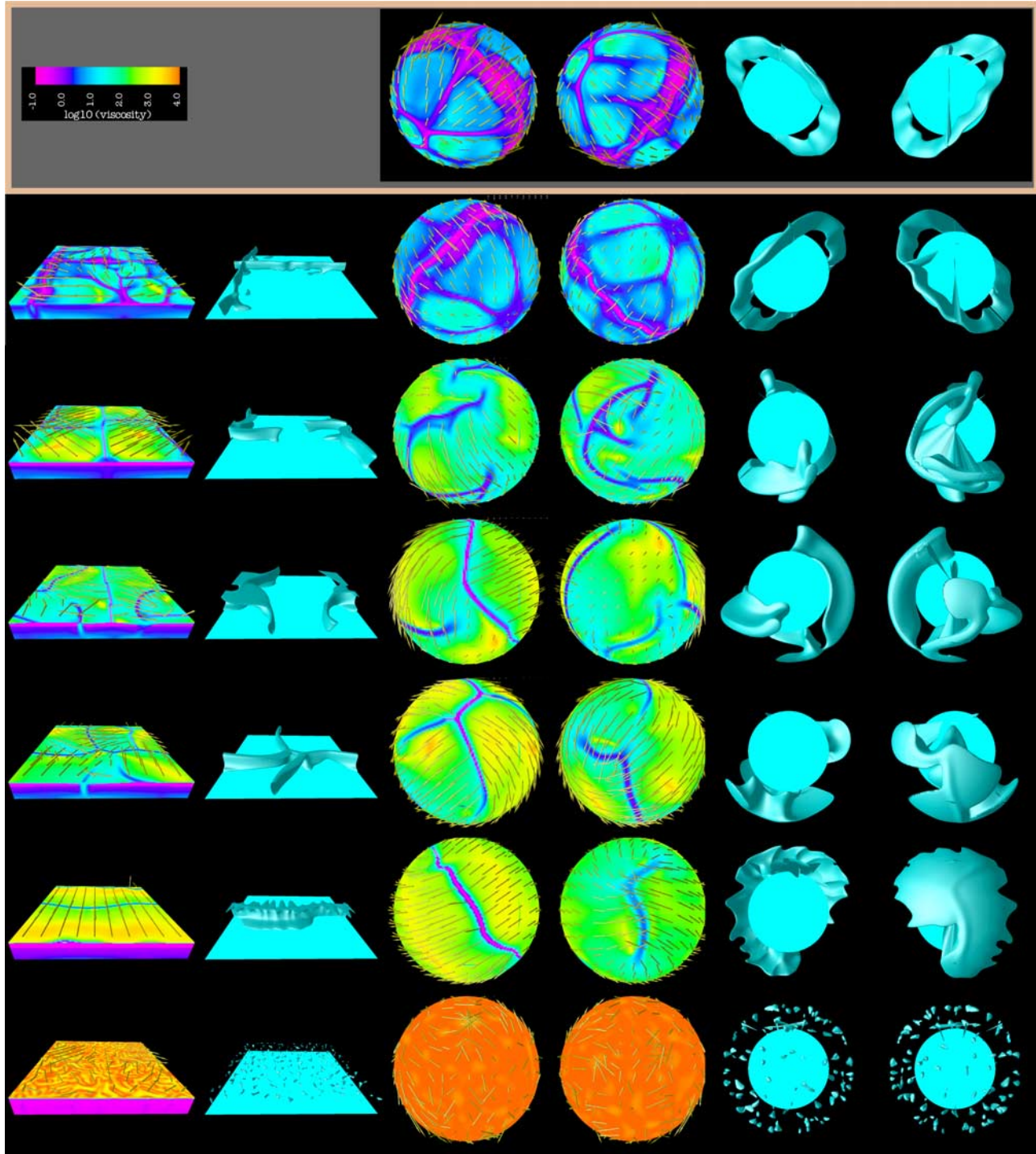


**Figure 1.** (left) The viscosity at the surface ( $z = 0.97$ ), arrows indicate the velocity field. The narrow blue/purple zones represent weak zones, i.e., plate boundaries. Orange/red zones indicate rigid zones, i.e., plates. (right) The temperature where it is 17% lower than the horizontal average. For the spherical cases both sides of the sphere are printed next to each other. Yield stress increases from top to bottom as;  $1.4 \cdot 10^3$ ,  $5.7 \cdot 10^3$ ,  $8.5 \cdot 10^3$ ,  $9.9 \cdot 10^3$ ,  $2.0 \cdot 10^4$ ,  $3.5 \cdot 10^4$ . The images show snapshots taken from each run. In the box at the top a snapshot similar to first calculation is shown but rotated arbitrarily.

results presented here give a crude approximation of plate tectonic regimes on terrestrial planets.

[30] Two new planforms are found. At the lowest lithospheric yield stresses ( $\sim 17$  MPa) one great circle downwelling forms. This separates the domain in two hemispheres

**Table 1.** Parameters for Dimensional Scaling

Quantity	Non-D Value	Dimensional Value
$\eta_0$	1	$10^{23}$ Pa s
$K$	1	$10^{-6}$ m <sup>2</sup> /s
$D$	1	$2.89 \times 10^6$ m

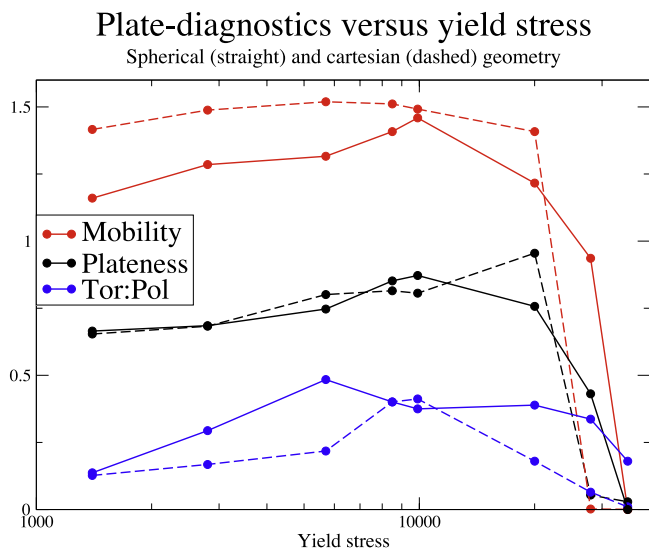


**Figure 2.** Values of the plate diagnostics versus yield stress. Spherical cases: solid lines, cartesian cases: dashed lines. Values were averaged over the second half of the run. For the x-axis a logarithmic scale is used. See text for discussion.

which each show several oceanic plates, separated by spreading centers. At high-intermediate lithospheric yield stresses ( $\sim 240$  MPa) two hemispherical plates form, separated by one elongated downwelling and one elongated upwelling.

[31] A major effect of spherical geometry is that the toroidal-poloidal ratio of the surface velocity field increases significantly compared to cartesian geometry. A wide range of lithospheric yield stresses give Earth like values.

[32] One distinction between the different observed regimes is the characteristic wavelength of convection. With increasing yield stress the convective wavelength changes from low (regime one) to high (regime two), to the highest possible (regime three) to very low in a rigid lid.

[33] This has several important implications for the planet. One is the cooling rate. As Grigné *et al.* [2005] showed, the surface heat flux depends on the wavelength of convection (in the mobile lid regime).

[34] Another implication will be in the efficiency of mixing. Since both the mixing time and the spatial scale of heterogeneities depends on the length scale of convection [Schmalzl and Hansen, 1994], the spatial scale of heterogeneities in the mantle is dictated by the present planform, as well as past planforms.

[35] Clearly, there are differences between real planets and models like these. Most notable are the absence of purely toroidal surface motion (strike-slip faults) and the formation of only double-sided subduction zones. The absence of purely toroidal surface motion is probably due to the way in which the yielding is implemented, i.e., via the (isotropic) second order invariant of the strain rate tensor. Tagawa *et al.* [2007] succeeded in producing single-sided subduction in a dynamical model by using a strongly history dependent rheology at the lubrication of plate boundaries. They did however, use a pre-set initial weak zone which evolved into the plate boundary. Gerya *et al.* [2008] showed

that dehydration and migration of water in regions of subduction stabilizes single-sided subduction, mainly through the formation of weak hydrated interplate shear zones.

[36] In order to get out of the rigid lid regime, we need yield stresses lower than  $\sim 420$  MPa. The estimated strength of oceanic lithosphere on Earth, based on laboratory experiments, is about 700 MPa [Kohlstedt *et al.*, 1995]; for lithosphere of 25 My old). All numerical studies on self consistent plate tectonics published to date show a similar discrepancy with the laboratory experiments. Only when pre-set weak zones are implemented (as by, for example, Tagawa *et al.* [2007]) numerical studies can match the values found by Kohlstedt *et al.* [1995]. One explanation might be found in the weakening effect of thermal cracking and hydration of oceanic lithosphere, as recently suggested by Korenaga [2007].

[37] There are several important things that need to be kept in mind when comparing the model to real planets. We modelled an incompressible, non-elastic fluid with no bottom heating and constant internal heat production, using the Boussinesq approximation and free slip boundary conditions on a fixed surface. Furthermore, the model does not incorporate continents. The effect of continents on tectonic planforms in spherical geometry is not known but the work of Grigné *et al.* [2007] and Zhong *et al.* [2007] suggest that it is significant. The Rayleigh number for the Earth is higher than the one used in the model. Higher Rayleigh number will lead to more vigorous convection. Preliminary results of calculations with  $Ra = 10^6$  (not shown) suggest that the basic planforms observed in the present study still form. Phase changes have an important effect on the convective patterns [e.g., Tackley *et al.*, 1993] but are not incorporated here. Their effect on tectonic planforms is unknown.

[38] In the present study we presented the different planforms possible on terrestrial planets. Future work will address questions such as the effect of different  $Ra$ , internal and bottom heating rate, surface heat flux scaling and coupled thermal and tectonic evolution of terrestrial planets. Grigné *et al.* [2005] showed the effect of convective wavelength on  $Nu - Ra$  scalings. As can be seen in Figure 1, the convective wavelength changes quite drastically between different planforms. This suggests that also the  $Nu - Ra$  scalings, and thus the cooling rate of the terrestrial planets, depend on the tectonic planform. A description of the tectonic planforms in 3D spherical geometry is a necessity to explain thermal evolution of terrestrial planets as well as to find criteria for (extrasolar) planets to have active plate tectonics.

[39] **Acknowledgments.** This research was supported by SNF. The authors are thankful for the reviews by Dave Yuen and Louis Moresi which improved the manuscript.

## References

- Bercovici, D. (2003), The generation of plate tectonics from mantle convection, *Earth Planet. Sci. Lett.*, 205, 107–121.
- Fowler, A., and B. O'Brien (2003), Lithospheric failure on Venus, *Proc. R. Soc. London, Ser. A*, 459, 2663–2704.
- Gerya, T. V., J. A. D. Connolly, and D. A. Yuen (2008), Why is terrestrial subduction one-sided?, *Geology*, 1(36), 43–46.
- Grigné, C., S. Labrosse, and P. J. Tackley (2005), Convective heat transfer as a function of wavelength: Implications for the cooling of the Earth, *J. Geophys. Res.*, 110, B03409, doi:10.1029/2004JB003376.

- Grigné, C., S. Labrosse, and P. J. Tackley (2007), Convection under a lid of finite conductivity: Heat flux scaling and application to continents, *J. Geophys. Res.*, *112*, B08402, doi:10.1029/2005JB004192.
- Kohlstedt, D. L., B. Evans, and S. Mackwell (1995), Strength of the lithosphere: Constraints imposed by laboratory experiments, *J. Geophys. Res.*, *100*(B9), 17,587–17,602.
- Korenaga, J. (2007), Thermal cracking and the deep hydration of oceanic lithosphere: A key to the generation of plate tectonics?, *J. Geophys. Res.*, *112*, B05408, doi:10.1029/2006JB004502.
- Lithgow-Bertelloni, C., and M. A. Richards (1993), Toroidal-poloidal partitioning of plate motions since 120 ma, *Geophys. Res. Lett.*, *20*(5), 375–378.
- Loddoch, A., C. Stein, and U. Hansen (2006), Temporal variations in the convective style of planetary mantles, *Earth Planet. Sci. Lett.*, *251*, 79–89.
- Moresi, L., and V. Solomatov (1995), Numerical investigation of 2D convection with extremely large viscosity variations, *Phys. Fluids*, *7*(9), 2154–2162.
- Moresi, L., and V. Solomatov (1998), Mantle convection with a brittle lithosphere: Thoughts on the global tectonic style of the Earth and Venus, *Geophys. J. Int.*, *133*, 669–682.
- Muhlhaus, H.-B., and K. Regenauer-Lieb (2005), Towards a self-consistent plate mantle model that includes elasticity: Simple benchmarks and application to basic modes of convection, *Geophys. J. Int.*, *163*, 788–800.
- Ogawa, M. (2003), Plate-like regime of a numerically modeled thermal convection in a fluid with temperature-, pressure-, and stress-history-dependent viscosity, *J. Geophys. Res.*, *108*(B2), 2067, doi:10.1029/2000JB000069.
- Richards, M. A., W.-S. Yang, J. R. Baumgardner, and H.-P. Bunge (2001), Role of a low-viscosity zone in stabilizing plate tectonics: Implications for comparative terrestrial planetology, *Geochem. Geophys. Geosyst.*, *2*(8), 1026, doi:10.1029/2000GC000115.
- Schmalzl, J., and U. Hansen (1994), Mixing the Earth's mantle by thermal convection: A scale dependent phenomenon, *Geophys. Res. Lett.*, *21*(11), 987–990.
- Solomatov, V. (1995), Scaling of temperature- and stress-dependent viscosity convection, *Phys. Fluids*, *7*, 266–274.
- Stein, C., J. Schmalzl, and U. Hansen (2004), The effect of rheological parameters on plate behaviour in a self-consistent model of mantle convection, *Phys. Earth Planet. Inter.*, *142*, 225–255.
- Tackley, P. J. (1993), Effects of strongly temperature-dependent viscosity on time-dependent, three-dimensional models of mantle convection, *Geophys. Res. Lett.*, *20*(20), 2187–2190.
- Tackley, P. J. (2000a), Self-consistent generation of tectonic plates in time-dependent, three-dimensional mantle convection simulations, *Geochem. Geophys. Geosyst.*, *1*(8), 1021, doi:10.1029/2000GC000036.
- Tackley, P. J. (2000b), Self-consistent generation of tectonic plates in time-dependent, three-dimensional mantle convection simulations, *Geochem. Geophys. Geosyst.*, *1*(8), 1026, doi:10.1029/2000GC000043.
- Tackley, P. J. (2008), Modelling compressible mantle convection with large viscosity contrasts in a three-dimensional spherical shell using the yinyang grid, *Phys. Earth Planet. Inter.*, in press.
- Tackley, P. J., D. J. Stevenson, G. A. Glatzmaier, and G. Schubert (1993), The effect of an endothermic phase transition at 670 km depth in a spherical model of convection in the Earth's mantle, *Nature*, *361*, 699–704.
- Tagawa, M., T. Nakakuki, M. Kameyama, and F. Tajima (2007), The role of history-dependent rheology in plate boundary lubrication for generating one-sided subduction, *Pure Appl. Geophys.*, *164*, 879–907.
- Trompert, R., and U. Hansen (1998), Mantle convection simulations with rheologies that generate plate-like behaviour, *Nature*, *395*, 686–689.
- Zhong, S., N. Zhang, Z.-X. Li, and J. H. Roberts (2007), Supercontinent cycles, true polar wander, and very long-wavelength mantle convection, *Earth Planet. Sci. Lett.*, *261*, 551–564.

---

P. J. Tackley and H. J. van Heck, Institute of Geophysics, ETH Zurich, Schafmattstrasse 30, CH-8093 Zürich, Switzerland. (hvanheck@erdw.ethz.ch; ptackley@ethz.ch)